Published in final edited form as:

Cell Rep. 2024 October 22; 43(10): 114744. doi:10.1016/j.celrep.2024.114744.

Daily oscillations of neuronal membrane capacitance

Daniel Severin[1,2], **Cristián Moreno**[1,2], **Trinh Tran**[1,2], **Christian Wesselborg**[3], **Sofia Shirley**[3], **Altagracia Contreras**[3], **Alfredo Kirkwood**[1,2,3,*], **Jorge Golowasch**[4,5,*]

[1]Johns Hopkins Zanvyl Krieger Mind/Brain Institute, Johns Hopkins University, Rm. 350 Dunning Hall, 3400 N. Charles St., Baltimore, MD 21218, USA

[2]The Solomon H. Snyder Department of Neuroscience, Johns Hopkins University, 3400 N. Charles St., Baltimore, MD 21218, USA

[3]Department of Biology, Johns Hopkins University, 3400 N. Charles St., Baltimore, MD 21218, USA

[4]Department of Biological Sciences, New Jersey Institute of Technology, Newark, NJ 07102, USA

[5]Lead contact

SUMMARY

Capacitance of biological membranes is determined by the properties of the lipid portion of the membrane as well as the morphological features of a cell. In neurons, membrane capacitance is a determining factor of synaptic integration, action potential propagation speed, and firing frequency due to its direct effect on the membrane time constant. Besides slow changes associated with increased morphological complexity during postnatal maturation, neuronal membrane capacitance is considered a stable, non-regulated, and constant magnitude. Here we report that, in two excitatory neuronal cell types, pyramidal cells of the mouse primary visual cortex and granule cells of the hippocampus, the membrane capacitance significantly changes between the start and the end of a daily light-dark cycle. The changes are large, nearly 2-fold in magnitude in pyramidal cells, but are not observed in cortical parvalbumin-expressing inhibitory interneurons. Consistent with daily capacitance fluctuations, the time window for synaptic integration also changes in pyramidal cells.

In brief

Severin et al. describe time-of-day changes in membrane capacitance in excitatory neurons from the visual cortex and hippocampus. Membrane capacitance is usually stable. These daily

*Correspondence: kirkwood@jhu.edu (A.K.), golowasch@njit.edu (J.G.).

AUTHOR CONTRIBUTIONS

D.S. designed and performed experiments and analyses and reviewed and edited the manuscript. C.M., T.T., C.W., S.S., and A.C. performed experiments and reviewed the manuscript. A.K. conceived the project, designed experiments, and wrote and edited the manuscript. J.G. conceived the project, designed experiments, performed analyses and computational experiments, and wrote and edited the manuscript.

DECLARATION OF INTERESTS

The authors declare no competing interests.

SUPPLEMENTAL INFORMATION

Supplemental information can be found online at https://doi.org/10.1016/j.celrep.2024.114744.

variations could profoundly impact neuronal physiology because of capacitance's influence on the membrane time constant. Consistent with this, the authors show strong changes in synaptic integration.

Graphical abstract

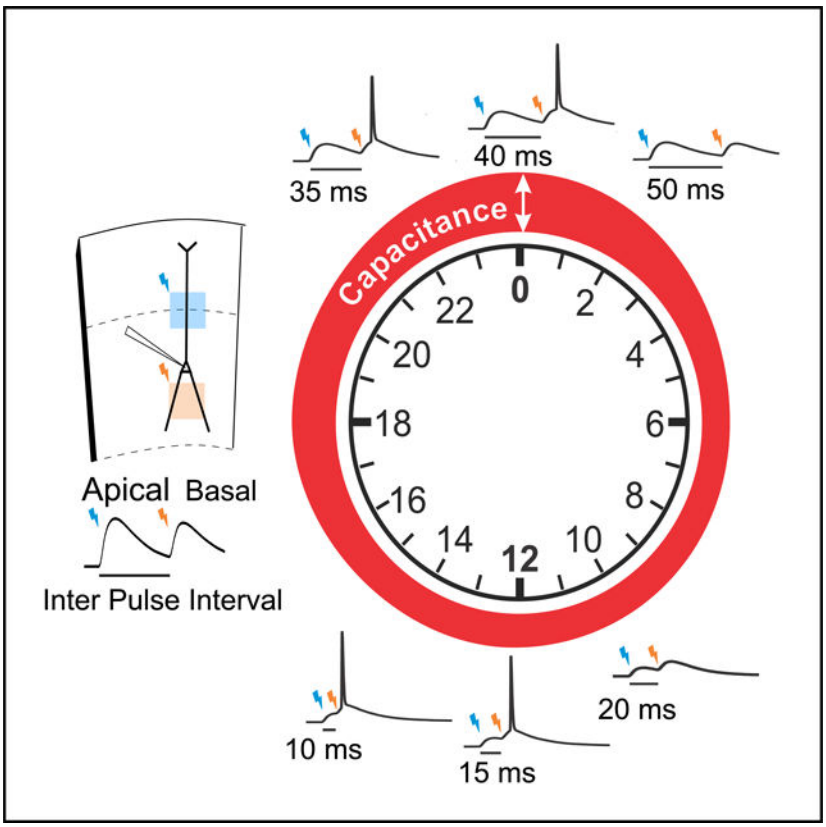

INTRODUCTION

Capacitance is a so-called passive property of the membrane and is a determining factor of fundamental neuronal properties, such as action potential propagation speed,[1] synaptic integration,[2,3] and action potential firing frequency.[4] As summarized in the following equation

$$C_m = \varepsilon \frac{A}{d}$$

(Equation 1)

capacitance depends not only on the dielectric constant (ε) of the insulating material (the phospholipid bilayer in biological membranes) but also on the distance between the intracellular and the extracellular conductive milieu (d) and the membrane area (A). In most neurons, total membrane capacitance increases as the membrane area increases during the maturation of structural complexity. In some neuronal types, the capacitance becomes

smaller as d increases due to myelin wrapping[5] or perineuronal net (PNN) encapsulation.[4] Because of its assumed stability, it is common practice to report changes in capacitance as a proxy for changes in membrane surface.[6–9] In juveniles and adults, altered capacitance has only been reported for some mouse models of some neurological conditions or after traumatic insult.[4,10–13] After maturation is completed, membrane capacitance is largely considered to be a constant biophysical property of the neurons and to be physiologically unregulated, since d and the properties of membrane lipids, captured by ε, are also thought to be stable.[14]

Here we report a 60%–100% daily oscillation of membrane capacitance in excitatory pyramidal cells of the mouse visual cortex from layers 2/3 and hippocampus dentate gyrus granule cells. In contrast, parvalbumin-positive (PV^+) inhibitory interneurons of the same visual cortex region show no such variations. We used an optogenetic approach to test the effect of such capacitance changes on the synaptic integration of inputs to apical and basal dendrites and confirmed the prediction that increased capacitance widens the synaptic integration window.

RESULTS

Membrane capacitance varies as a function of time of day

We evaluated daily changes in membrane capacitance, C_m, in three types of identified neurons: pyramidal cells (Figure 1A) and PV^+ inhibitory neurons (Figure 1C) located in layers 2/3 of the primary visual cortex and granule cells (GCs) from the hippocampus dentate gyrus (Figure 1B). In each case, C_m was calculated from current-clamp measurements of the membrane time constant, which was determined with multi-exponential fits to current pulse-induced voltage responses as described in STAR Methods (Figure 1D). Surprisingly, we observed a large C_m decrease from the end of the dark/beginning of the light period (Zeitgeber Time 0, ZT0) to the middle (ZT6) and end (ZT12) of the light period in pyramidal cells (Figure 2A, left). In hippocampal GCs, we also observed a large and significant C_m decrease between ZT0 and ZT12 (Figure 2A, center). These changes are highly statistically significant in both cell types (Figure 2; Table S1).

Since pyramidal and GCs are both excitatory, we asked whether the total membrane capacitance of identified inhibitory cells might also vary as a function of the time of day. Previous work has shown small but significant daily changes in PNN wrapping around PV^+ inhibitory cells in many brain areas, including the cortex and hippocampus, that could result in membrane capacitance changes.[15] We recorded the time constant and calculated total C_m in identified inhibitory PV^+ neurons from layers 2 and 3 of the visual cortex. In contrast to the excitatory neurons, cortical inhibitory PV^+ neurons did not show any significant membrane capacitance change during the course of a 24-h day/light cycle (Figure 2A, right; Table S1).

We observed a similar time-of-day dependence of the time constant, τ_m, that closely tracks the membrane capacitance changes in both cortical pyramidal and hippocampal GCs (Figure 2B). The changes of τ_m with the time of day were statistically significant (Table S2), with

the main differences arising from differences between ZT0–ZT12 and ZT6–ZT18 ($p < 0.05$; Figure 2B, left) for pyramidal cells. However, as with C_m, τ_m did not significantly vary in PV^+ neurons (Figure 2B, right; Table S2).

Finally, τ_m is the product of the membrane capacitance and the membrane resistance, R_m (Equation 1). Therefore, we calculated R_m (the resistive component of the exponential term that yields τ_m[16]) in all three cell types to examine to what extent it may affect the temporal properties of the membrane in these cells. We observed that only in pyramidal cells is there a significant effect of time of day on R_m (Figure 2C, left; Table S3). Both GCs and PV^+ cells show no significant R_m changes (Figure 2C, center and right; Table S3). Importantly, the R_m changes observed in pyramidal cells run opposite to the changes in membrane time constant and capacitance (Figure 2C, left), suggesting that τ_m changes are primarily due to membrane capacitance and not membrane resistance changes.

These results are unexpected, as the membrane capacitance is normally thought to be very stable. These changes are expected to have a number of functional consequences, which we explore below. We first examine the possible role of PNNs in driving (or occluding) these changes.

Role of PNNs in regulating membrane capacitance changes

Our observation that C_m in PV^+ interneurons seemingly does not change during the day raised the possibility that daily changes in PNNs[15] might mask intrinsic capacitance changes in these cells. We used chondroitinase ABC from *Proteus vulgaris* (ChABC; STAR Methods) to digest the PNN and measured the capacitance in the treated PV^+ neurons. Nearly all PV^+ cells in the visual cortex express high levels of *Wisteria floribunda* agglutinin (WFA)-positive staining surrounding their somata and proximal dendrites (Figure 3A). Similarly, nearly all PV^+ cells lose all visible evidence of the presence of PNNs (no WFA green staining after treatment with ChABC, which is known to disrupt PNNs) (Figure 3B). Yet, the lack of difference in membrane capacitance between ZT0 and ZT12 observed in control PV^+ neurons (Figure 2A, right) remains unchanged (Figure 3C). This leads us to conclude that PNNs are unlikely to be responsible for occluding or significantly affecting any membrane capacitance changes that PV^+ cells might express. The results do not exclude the participation of other extracellular matrix components in the regulation of capacitance observed in cortical pyramidal and hippocampal GCs but clearly indicate that inhibitory PV^+ neurons do not express such regulation.

Functional consequences

The unexpected variation in membrane capacitance throughout the day prompted us to evaluate whether the larger C_m at ZT0, and, thus, longer time constant, translates into a larger temporal window for integrating excitatory inputs. To that end, we tested whether pyramidal cells better integrate, at ZT0, two subthreshold excitatory inputs separated in time and space (Figure 4A). In these experiments, performed in slices of Emx1-cre; Ai32 mice expressing ChR2 in excitatory neurons, two square subthreshold light stimuli were applied sequentially: one above (mimicking apical inputs) and the other below the soma (mimicking basal inputs) of the recorded pyramidal cell (Optical stimulation). The inter-pulse intervals (IPI) were

systematically varied from 5 to 60 ms. We expected that the larger the capacitance, and, thus, the time constant, the longer the effective integration time window would be; i.e. the longer the IPI that effectively induces firing in the cell after the basal dendrite was activated. Figure 4 confirms this prediction. The capacitance (and time constant) at ZT0 is longer (Figure 2A, left), and, thus, longer IPIs were able to induce spiking in ZT0 cells (Figure 4B, blue traces) compared to ZT12 cells (Figure 4B, orange traces). Figure 4C summaries these observations by showing the fraction of all cells tested in each condition that fired at least one action potential after the indicated IPIs. The ZT0 cells show a significantly larger fraction of cells firing than ZT12 cells at each IPI tested (two-way ANOVA, $p < 0.0001$).

A simplified computational model of a pyramidal cell (Figure 4D) confirmed that increases in capacitance are sufficient to increase the window for temporal integration of distinct inputs (Figures 4D–4F). In the simplified (cartoon) model pyramidal cell, each dendrite was stimulated with a synapse at its center with subthreshold synaptic conductance as in the experimental case (STAR Methods). The results very closely mimic the experimental observations, with the curves separated by approximately 25 ms for a 2-fold change in capacitance (and, thus, time constant).

These results strongly suggest that integration of inputs from different regions feeding into the main excitatory neurons in the visual cortex is likely to greatly vary between day and night.

DISCUSSION

Here, we report that the membrane capacitance in two types of excitatory neurons, visual cortex pyramidal cells and hippocampus GCs, exhibits a surprising daily oscillation (exceeding 60% change between peak and trough). These changes occur with a maximum around ZT0 (end of the dark phase/beginning of the light phase) and a minimum around ZT6–ZT12 (middle to end of the light phase). In contrast, membrane capacitance did not change in visual cortical PV^+ inhibitory neurons. Thus, in a manner highly reminiscent of our recent report of large daily changes in excitation/inhibition balance,[17] the capacitance changes are not restricted to a single brain region, yet, within a region, they do not occur in all neuron types. Together, both observations reveal an unexpected degree of complex neural remodeling in fundamental membrane properties previously considered stable. The amplitude of the membrane capacitance changes is surprising, exceeding by almost an order of magnitude membrane capacitance changes observed in previous studies.[4,10–13]

Multiple independent cellular mechanisms could potentially contribute to the daily modulation of capacitance. One candidate could be daily changes in membrane area resulting from the turnover of cortical synaptic spines, which are known to exhibit a circadian-like regulation of number and shape.[18,19] However, surface changes alone are highly unlikely to account for the 60%–100% daily change in total membrane capacitance reported here, since these synaptic changes affect a relatively small fraction of spines. Similarly, the dendritic arborization of pyramidal neurons in the mouse visual cortex can increase substantially in length and complexity, but only for a short postnatal period in a process that is nearly completed by post-natal day 21 (P21) in V1, which is the age of the

youngest of our subjects.[20] Furthermore, dendritic length and number changes as a function of visual experience are much smaller than the observed C_m changes.[20]

Another possibility to consider is the recent report that conditioning artificial phospholipid membranes with voltage stimulation induces persistent, yet reversible, changes in the area and thickness of artificial bilayers, therefore affecting their capacitance.[21] If this mechanism also operates in the brain, then the changes in membrane capacitance would be expected to reflect daily oscillations in total neuronal activity.

A perhaps more plausible mechanism relates to changes in the extracellular space (ECS) volume and extracellular matrix (ECM) organization. Consider a simple scenario in which current injected into a neuron sequentially crosses its own membrane, then an ECS of variable thickness and a layer of glial membrane and/or specialized ECM,[22] to finally reach the reference electrode. In that case, the estimated C_m strongly depends on the ECS width, as it would impact the effective d (Equation 1). This scenario would predict local but extensive changes in ECS around cortical pyramidal and hippocampal GCs, with ECS expanding (or ECM changing composition) during the light phase (when C_m drops) and shrinking during the dark phase (inducing C_m increases). The changes would need to be local since, otherwise, they would not explain the lack of C_m change in PV^+ interneurons. One form of specialized ECM that has been shown to affect membrane capacitance around epileptic foci is the PNN that prominently encapsulates PV^+ interneurons[4,23,24] (Figure 3A). One intriguing possibility we considered is the idea that the unique C_m stability in PV^+ interneurons relates to their tight encapsulation by PNNs, perhaps related to the loss of neuronal plasticity thought to be due to PNN encapsulation.[23,25] This is not supported by our experimental observations (Figure 3). We found that dissolving the PNNs surrounding cortical PV^+ cells with ChABC (Figure 3B) does not modify the capacitance levels (Figure 3C) observed under control conditions (Figure 2A) at ZT0 and ZT12. It is important to point out that PNNs are not observed in either cortical pyramidal or hippocampal GCs.[4,24,26] Thus, this particular form of ECM cannot be part of the mechanism that gives rise to the observed changes.

Membrane capacitance changes can profoundly impact the physiology of the affected neurons and the networks they are part of through their effects on the membrane time constant. Three principal effects that changes in the capacitance and time constant of a neuron can have are changes in synaptic integration, changes in action potential propagation speed, and changes in action potential generation frequency. We tested the effect on synaptic integration experimentally and computationally and found that the changes in capacitance that we measured greatly affects the window of input integration, with a larger capacitance and time constant during the dark phase significantly increasing this window (Figure 4).

Synaptic integration is likely the most consequential of the functional effects that capacitance changes can have because it plays a crucial role in the computation of inputs coming from different regions of the nervous system onto a target cell.[27] Layer 2/3 pyramidal cells receive information from both top-down C, with apical and basal dendrites handling these incoming signals, respectively. They are thus key integrators of activity within the cortex and between cortex and basal ganglia. The integration of these inputs, and, thus, the resulting pyramidal cell output, is strongly affected by the relative timing

of their arrival and by the membrane time constant.[28] Similarly, GCs receive inputs from the lateral and medial entorhinal cortices in the upper and lower portions of the perforant path, respectively. In addition, C_m changes will likely alter the velocity and reach of action potentials back-propagating into apical dendrites. In turn, this can affect the modification of distal synapses induced via spike timing-dependent plasticity (STDP), because STDP depends crucially on the coincidence of synaptic activation with the arrival of the action potential.[29]

The exact consequences of daily C_m changes in the function of actual neural circuits are not simple to predict because they likely occur in the context of multiple other daily neuronal changes, such as those affecting ion conductance regulation,[30] co-regulation of active conductance,[31] and regulation of the excitation/inhibition balance.[17] Whether these various processes compensate or amplify the consequences of membrane capacitance changes remains to be determined. In either case, we propose that the observation of large daily membrane capacitance changes introduces a fundamental variable that needs to be considered for understanding the dynamics of neuronal activity.

Limitations of the study

The results of this study show clear daily fluctuations in neuronal C_m, yet the potential contribution of multiple plausible cellular mechanisms remains to be determined.

Also unclear is the prevalence of the phenomenon. Do other excitatory cells also exhibit daily oscillations in C_m, and is C_m constant in other types of interneurons? Finally, another aspect that needs further examination is functional consequences. This is because besides affecting input integration, changes in C_m also affect firing rates and firing delays. Indeed, how these potential daily changes could influence the dynamics of cortical networks remains an open question.

In this study, while assessing the functional significance of the capacitance changes that we discovered, we decided to purposefully not block or inhibit any voltage-gated currents to keep the cells as close to intact as possible. It is unlikely, but possible, that a similar functional effect of capacitance changes can be produced by changes in voltage-gated ionic currents. Preliminary modeling results (unpublished data) suggest that this is very unlikely, but it remains to be fully tested.

STAR★METHODS

RESOURCE AVAILABILITY

Lead contact—Requests for further information, resources, and reagents should be directed to and will be fulfilled by the lead contact, Jorge Golowasch (golowasch@njit.edu).

Materials availability—No new biological materials were generated during this study.

Data and code availability

- Data are available upon request.

- The model built during this study can be found in https://github.com/golowasch/Pyramidal_ball-2-sticks.
- Any additional information required to reanalyze the data reported in this work paper is available from the lead contact upon request.

EXPERIMENTAL MODEL AND STUDY PARTICIPANT DETAILS

Both male and female animals were used. For visual cortex neuronal recordings we used 20–26 days old PV-cre; Ai14 mice (RRID:IMSR_JAX:008069) from Jackson Laboratories, Bar Harbor, Main, USA.

For hippocampal neuronal recordings we used 114–128 days (~4 months) old C57BL/6 mice (RRID:IMSR_JAX:000664) from Jackson Laboratories, Bar Harbor, Maine, USA.

To test synaptic integration, we generated double transgenic animals crossing the Emx1-Cre mouse line (RRID:IMSR_JAX:005628) with the Ai32 mouse line (RRID:IMSR_JAX:012569) that has a conditional allele of Rosa-CAG-LSL-ChR2(H134R)-EYFP-WPRE to drive ChR2/EYFP fusion protein expression in principle cells (all mice from Jackson Laboratories, Bar Harbor, Maine, USA).

All experiments were performed in accordance with the U.S. Public Health Service Policy on Humane Care and Use of Laboratory Animals, the National Institutes of Health Guidelines for the Care and Use of Animals in Research and approved by the Institutional Animal Care and Use Committee at Johns Hopkins University, where the recordings were performed.

We observed no significant effects of sex on our results. However, the number of samples is limited when the sexes are segregated at each ZT, and this remains a limitation of this study that deserves future examination.

METHOD DETAILS

Animal light entrainment and slice preparation—Mice were “entrained” for ≥2 weeks with 12-h light/dark cycles. For slice preparations, the mice were removed from their cages ~10 min before the chosen circadian time of study (*Zeitgeber*, ZT = 0/24, 6, 12 or 18 h). The mice were first deeply anesthetized with isofluorane within 10 min after removal from their cages and then perfused transcardially with cold dissection buffer (5 mL at 10 mL/min) containing 212.7 mM sucrose, 5.0 mM KCl, 0.5 mM CaCl2,10 mM MgSO4 1.25 mM NaH2PO4, 26 mM NaHCO3, and 10 mM glucose. After decapitation, brains were quickly removed, and acute sagittal brain ~300 μm thick slices were made for visual cortex slices, and hippocampal slices (also ~300 μm thick) were made as described in,[32] both in ice-cold dissection buffer bubbled with a mixture of 5% CO2 and 95% O2. The slices were allowed to recover for 30 min at 30°C in dissection buffer and then for 30 min at room temperature in artificial cerebrospinal fluid (ACSF): 124 mM NaCl, 5 mM KCl, 1.25 mM NaH2PO4, 26 mM NaHCO3, 1.5 mM MgCl2, 2.5 mM CaCl2, and 10 mM dextrose, and bubbled with a mixture of 5% CO2 and 95% O2.

All recordings were performed in a submerged recording chamber superfused with ACSF (30 ± 0.5°C, 2 mL/min). Synaptic blockers were included in the bath: 25 μM 6-cyano-7-nitroquinoxaline-2,3-dione (CNQX) to block AMPA/kainate receptors, 100 μM DL-2-amino-5 phosphonopentanoic acid (APV) to block NMDA receptors, and 10 μM gabazine to block GABAA receptors. Whole-cell voltage-clamp recordings were obtained from pyramidal cells identified by their shape and firing response to depolarizing current pulses (Figure 1A) in cortical layers 2 and 3, and from identified parvalbumin (PV) cells (fluorescent in PV-cre; Ai14 mice). Hippocampal granule cells (GCs) were identified by their shape and position in the upper blade of the dentate gyrus (DG). We used borosilicate glass patch pipettes (3–6 MΩ) filled with intracellular solution containing the following: 130 mM K-gluconate, 10 mM KCl, 0.2 mM EGTA, 10 mM HEPES, 4 mM MgATP, 0.5 mM Na3GTP, 10 mM Na-phosphocreatine (pH 7.2–7.3, 280–290 mOsm). Average input resistance of pyramidal cells was 81.9 ± 21.7 MΩ (range: 64.4 to 115.0 MΩ), of PV cells was 148.7 ± 41.3 MΩ (range: 51.2 to 306.0 MΩ), and of granule cells was 249.2 ± 79.9 MΩ (range: 153.0 to 512.8.0 MΩ). Series resistance was <20 MΩ (range 6–20MΩ), which was compensated at least 80% in every case. All drugs were purchased from either Sigma Aldridge (RRID:SCR_008988) or Tocris (RRID:SCR_003689).

Capacitance measurements—Membrane capacitance was measured as described in Golowasch et al.[16] using current clamp pulses, which we showed give a better approximation to the actual total membrane capacitance that voltage clamp methods. We used small depolarizing or hyperpolarizing current pulses from a voltage around the resting potential of the cells (Resting potentials: Pyramidal cells: −70.2 ± 6.5 mV, $N = 39$; PV^+ cells: −63.9 ± 5.2 mV, $N = 45$; GCs: −64.0 ± 8.6 mV, $N = 30$). The rationale for the chosen baseline voltage and the pulse amplitude was to avoid or minimize entering a voltage range where voltage-dependent currents are activated during the pulse,[33] thus remaining within levels where the cells respond passively. 1 second-long pulses were repeated at least 5 times, averaged to reduce noise and then baseline subtracted. We used a window of around the first 250 ms and fitted the resulting trace with a double exponential function starting 0.5–1 msec after the onset of the pulse, thus avoiding the initial Rs-driven membrane potential transient (Figure 1D). The slowest exponential component corresponds to the cell's membrane charging curve,[34] from which the time constant (τ_m) can be obtained, and the total membrane capacitance (C_m) and the total membrane resistance (R_m) can be calculated.[16,34] Note that R_m is derived from the amplitude of this slow exponential component and is not the same as the input resistance, R_{input}, of the cell.[16,34] In practice, it was typical that a much slower time constant arose from this procedure due to small amounts of noise or drift, in which case we used the second exponential component parameters. To ensure the use of healthy cells, we used pyramidal cells with $R_{input} \geq 100$MΩ, granule cells with $R_{input} \geq 80$MΩ, and PV^+ cells with $R_{input} \geq 50$MΩ.

Optical stimulation—A 470 nm digital micromirror device (Polygon, Mightex) was used to excite channelrhodopsin 2 (ChR2) in visual cortex pyramidal cells of 8 mice. The light was delivered to the top of the slice through a Nikon LWD 16x/0.80w objective of a Nikon Eclipse E600FN microscope. The 3 msec-long light pulses covered a square of 65 × 65 μm^2 on each dendrite (see Figure 4A) and were applied every 15 s, first to the apical then to the

basal dendrite separated by a varying inter-pulse-interval (IPI). Importantly, 10 μM CNQX, 10 μM APV, and 10 μM Gabazine were added to the ACSF to prevent unintended synaptic activation from off-target sources. To quantify input integration, we used sub-threshold intensities for both ChR2-activated conductances calculated as follows: we measured the slope of the light-induced response 3 msec after initiating the light pulse. We identified the slope of the smallest response that could generate an action potential separately in each dendrite (threshold slope). We then used light intensities to stimulate each dendrite at 80% of the threshold slope. Finally, we determined the maximal apical-basal IPI that triggered an action potential in cells from ZT0 and ZT12-entrained mice. We repeated this several times at each IPI for each cell and determined the fraction of times each cell fired at least one action potential (Figure 4B). The values on Figure 4C correspond to the average of firing across multiple cells.

Modeling—A simplified compartmentalized conductance-based pyramidal cell model was built using MATLAB (R2023b, MathWorks), which can be found in https://github.com/golowasch/Pyramidal_ball-2-sticks. All parameters used to build a cell can be found in the file cell_parameters_v3.m, and all conductance equations can be found in https://github.com/golowasch/Pyramidal_ball-2-sticks/blob/main/biophys_eqs_v3.m. The essence of the model cell is as follows: a 15μm diameter spherical soma is connected to one apical (180 μm long, 2 μm diameter) and one basal dendrite (150 μm long, 2 μm diameter) (Figure 4D). The specific membrane resistance was adjusted to yield an input resistance of 116 MΩ. Only the soma was endowed with active properties: Hodgkin-Huxley-type equations for a voltage-gated Na^+ (I_{Na}) and a voltage-gated delayed rectifier K^+ current (I_{Kd}). The threshold for action potential firing (~−40mV) and firing frequency at rheobase of around 20 Hz, which is what we (Figure 1A) and others have observed[35]) were set by adjusting several parameters of I_{Na} and I_{Kd} (Figure 4D). After adjusting these parameters, we set the specific membrane capacitance to yield membrane time constants comparable to the maxima and minima we measured (Figure 1A, left). One synapse was placed on the apical (syn1) and one on the basal dendrite (syn2) at a position approximately equivalent to those used for our optical stimulation experiments (Figure 4A), *i.e.*, ~50% of the length of each dendrite (Figure 4D). We reproduced light-activated ChR2 (apical dendrite first) with a synaptic current following an alpha function with time constant 5 msec and reversal potential 0 mV and adjusted the synaptic conductance in exactly the same way as for the adjustment of light intensity for the biological experiments (previous section). To simulate the variability in the threshold voltage of the biological cells, we randomly increased or decreased by a maximum of 5% the half-maximal activation voltage of both I_{Na} (i.e. max ±1.65mV) and I_{Kd} (i.e. max ±0.8mV) in each run.

Chondroitinase treatment, staining and confocal imaging—A set of slices was treated for 45 min with chondroitinase ABC from *Proteus vulgaris* (ChABC, Sigma, St. Louis; Cat# C3667) together with a group of control slices obtained from the same litter of animals. Treatment was conducted after a recovery of 45 min post-slicing in 0.5 U ChABC 0.001% Bovine Serum Albumin (Fisher BioReagents; Cat# 9048–46-8) at 33 ± 0.5°C followed by patch clamping to measure membrane capacitance and then fixation with 0.4% paraformaldehyde overnight at 4°C. Slices were then washed in blocking solution

(normal goat serum in phosphate buffer (PBS) for 60 min at room temperature on a gentle rocker and then placed for 6 h at room temperature in fluorescein-conjugated *Wisteria Floribunda* Lectin (WFA, Vector Laboratories, FL-1351) under gentle rocking. Slices were finally washed 3 times in PBS for 10 min each and mounted on glass slides in ProLong Gold Antifade Mountant (Life Technologies). The PV-cre; Ai14 mouse strain expresses td-Tomato in all cortical PV^+ cells. We imaged the slices with a Leica SP8 confocal microscope (excitation 554 nm, emission: 581 nm, red staining) and WFA (excitation 495 nm, emission 515 nm, green) (Figures 3A and 3B). Each slice was imaged over 9 optical sections, each ~1 μm thick, and images show the collapsed z stack.

QUANTIFICATION AND STATISTICAL ANALYSIS

Data were statistically compared with one-way or two-way ANOVA tests for independent samples when normally distributed and non-normally distributed data were compared using Kruskal-Wallis ANOVA or Mann-Whitney Rank Sum *t* test. These statistical analyses were performed using SigmaStat and graphs were made with SigmaPlot (Systat Software, Inc., San Jose, CA. USA; RRID:SCR_010285) and CorelDraw (Corel Inc., Austin, TX, RRID:SCR_014235).

Figures show means and standard deviations unless otherwise indicated, and detailed statistical data are listed in Tables S1–S3.

Supplementary Material

Refer to Web version on PubMed Central for supplementary material.

ACKNOWLEDGMENTS

This work was supported by NIH grant 5R01-EY12124 (to A.K.) and NSF 2320895 (to J.G.). We thank Maya Golowasch for assistance with figure design.

REFERENCES

1. Hodgkin AL, and Huxley AF (1952). A quantitative description of membrane current and its application to conduction and excitation in nerve. J. Physiol. 117, 500–544. 10.1113/jphysiol.1952.sp004764. [PubMed: 12991237]
2. Martin AR (1976). The effect of membrane capacitance on non-linear summation of synaptic potentials. J. Theor. Biol. 59, 179–187. 10.1016/s0022-5193(76)80031-8. [PubMed: 181641]
3. Baufreton J, Atherton JF, Surmeier DJ, and Bevan MD (2005). Enhancement of excitatory synaptic integration by GABAergic inhibition in the subthalamic nucleus. J. Neurosci. 25, 8505–8517. 10.1523/JNEUROSCI.1163-05.2005. [PubMed: 16162932]
4. Tewari BP, Chaunsali L, Campbell SL, Patel DC, Goode AE, and Sontheimer H (2018). Perineuronal nets decrease membrane capacitance of peritumoral fast spiking interneurons in a model of epilepsy. Nat. Commun. 9, 4724. 10.1038/s41467-018-07113-0. [PubMed: 30413686]
5. Castelfranco AM, and Hartline DK (2015). The evolution of vertebrate and invertebrate myelin: a theoretical computational study. J. Comput. Neurosci. 38, 521–538. 10.1007/s10827-015-0552-x. [PubMed: 25832903]
6. Haedo RJ, and Golowasch J (2006). Ionic mechanism underlying recovery of rhythmic activity in adult isolated neurons. J. Neurophysiol. 96, 1860–1876. 10.1152/jn.00385.2006. [PubMed: 16807346]

7. Royeck M, Horstmann MT, Remy S, Reitze M, Yaari Y, and Beck H (2008). Role of axonal NaV1.6 sodium channels in action potential initiation of CA1 pyramidal neurons. J. Neurophysiol. 100, 2361–2380. 10.1152/jn.90332.2008. [PubMed: 18650312]
8. Pineda RH, Knoeckel CS, Taylor AD, Estrada-Bernal A, and Ribera AB (2008). Kv1 potassium channel complexes in vivo require Kvbeta2 subunits in dorsal spinal neurons. J. Neurophysiol. 100, 2125–2136. 10.1152/jn.90667.2008. [PubMed: 18684900]
9. Perez-Garcia P, Pardillo-Diaz R, Geribaldi-Doldan N, Gomez-Oliva R, Dominguez-Garcia S, Castro C, Nunez-Abades P, and Carrascal L (2021). Refinement of Active and Passive Membrane Properties of Layer V Pyramidal Neurons in Rat Primary Motor Cortex During Postnatal Development. Front. Mol. Neurosci. 14, 754393. 10.3389/fnmol.2021.754393. [PubMed: 34924951]
10. Amzica F, and Neckelmann D (1999). Membrane capacitance of cortical neurons and glia during sleep oscillations and spike-wave seizures. J. Neurophysiol. 82, 2731–2746. 10.1152/jn.1999.82.5.2731. [PubMed: 10561441]
11. Akopian G, Barry J, Cepeda C, and Levine MS (2016). Altered membrane properties and firing patterns of external globus pallidus neurons in the R6/2 mouse model of Huntington's disease. J. Neurosci. Res. 94, 1400–1410. 10.1002/jnr.23889. [PubMed: 27618125]
12. Perez H, Abdallah MF, Chavira JI, Norris AS, Egeland MT, Vo KL, Buechsenschuetz CL, Sanghez V, Kim JL, Pind M, et al. (2021). A novel, ataxic mouse model of ataxia telangiectasia caused by a clinically relevant nonsense mutation. Elife 10, e64695. 10.7554/eLife.64695. [PubMed: 34723800]
13. Rangel-Barajas C, Boehm SL, 2nd, and Logrip ML, (2021). Altered excitatory transmission in striatal neurons after chronic ethanol consumption in selectively bred crossed high alcohol-preferring mice. Neuropharmacology 190, 108564. 10.1016/j.neuropharm.2021.108564. [PubMed: 33857521]
14. Gentet LJ, Stuart GJ, and Clements JD (2000). Direct measurement of specific membrane capacitance in neurons. Biophys. J. 79, 314–320. 10.1016/S0006-3495(00)76293-X. [PubMed: 10866957]
15. Pantazopoulos H, Gisabella B, Rexrode L, Benefield D, Yildiz E, Seltzer P, Valeri J, Chelini G, Reich A, Ardelt M, and Berretta S (2020). Circadian Rhythms of Perineuronal Net Composition. eNeuro 7. 10.1523/ENEURO.0034-19.2020.
16. Golowasch J, Thomas G, Taylor AL, Patel A, Pineda A, Khalil C, and Nadim F (2009). Membrane capacitance measurements revisited: dependence of capacitance value on measurement method in nonisopotential neurons. J. Neurophysiol. 102, 2161–2175. 10.1152/jn.00160.2009. [PubMed: 19571202]
17. Bridi MCD, Zong FJ, Min X, Luo N, Tran T, Qiu J, Severin D, Zhang XT, Wang G, Zhu ZJ, et al. (2020). Daily Oscillation of the Excitation-Inhibition Balance in Visual Cortical Circuits. Neuron 105, 621–629.e4. 10.1016/j.neuron.2019.11.011. [PubMed: 31831331]
18. de Vivo L, Bellesi M, Marshall W, Bushong EA, Ellisman MH, Tononi G, and Cirelli C (2017). Ultrastructural evidence for synaptic scaling across the wake/sleep cycle. Science 355, 507–510. 10.1126/science.aah5982. [PubMed: 28154076]
19. Diering GH, Nirujogi RS, Roth RH, Worley PF, Pandey A, and Huganir RL (2017). Homer1a drives homeostatic scaling-down of excitatory synapses during sleep. Science 355, 511–515. 10.1126/science.aai8355. [PubMed: 28154077]
20. Richards SEV, Moore AR, Nam AY, Saxena S, Paradis S, and Van Hooser SD (2020). Experience-Dependent Development of Dendritic Arbors in Mouse Visual Cortex. J. Neurosci. 40, 6536–6556. 10.1523/JNEUROSCI.2910-19.2020. [PubMed: 32669356]
21. Scott HL, Bolmatov D, Podar PT, Liu Z, Kinnun JJ, Doughty B, Lydic R, Sacci RL, Collier CP, and Katsaras J (2022). Evidence for long-term potentiation in phospholipid membranes. Proc. Natl. Acad. Sci. USA 119, e2212195119. 10.1073/pnas.2212195119. [PubMed: 36469762]
22. Spijker S, Koskinen MK, and Riga D (2020). Incubation of depression: ECM assembly and parvalbumin interneurons after stress. Neurosci. Biobehav. Rev. 118, 65–79. 10.1016/j.neubiorev.2020.07.015. [PubMed: 32687884]

23. Wang D, and Fawcett J (2012). The perineuronal net and the control of CNS plasticity. Cell Tissue Res. 349, 147–160. 10.1007/s00441-012-1375-y. [PubMed: 22437874]
24. Briones BA, Pisano TJ, Pitcher MN, Haye AE, Diethorn EJ, Engel EA, Cameron HA, and Gould E (2021). Adult-born granule cell mossy fibers preferentially target parvalbumin-positive interneurons surrounded by perineuronal nets. Hippocampus 31, 375–388. 10.1002/hipo.23296. [PubMed: 33432721]
25. Carstens KE, Lustberg DJ, Shaughnessy EK, McCann KE, Alexander GM, and Dudek SM (2021). Perineuronal net degradation rescues CA2 plasticity in a mouse model of Rett syndrome. J. Clin. Invest. 131, e137221. 10.1172/JCI137221. [PubMed: 34228646]
26. Carceller H, Gramuntell Y, Klimczak P, and Nacher J (2023). Perineuronal Nets: Subtle Structures with Large Implications. Neuroscientist 29, 569–590. 10.1177/10738584221106346. [PubMed: 35872660]
27. Spruston N (2008). Pyramidal neurons: dendritic structure and synaptic integration. Nat. Rev. Neurosci. 9, 206–221. 10.1038/nrn2286. [PubMed: 18270515]
28. Jordan R, and Keller GB (2020). Opposing Influence of Top-down and Bottom-up Input on Excitatory Layer 2/3 Neurons in Mouse Primary Visual Cortex. Neuron 108, 1194–1206.e5. 10.1016/j.neuron.2020.09.024. [PubMed: 33091338]
29. Debanne D, and Inglebert Y (2023). Spike timing-dependent plasticity and memory. Curr. Opin. Neurobiol. 80, 102707. 10.1016/j.conb.2023.102707. [PubMed: 36924615]
30. Adamsky A, Kol A, Kreisel T, Doron A, Ozeri-Engelhard N, Melcer T, Refaeli R, Horn H, Regev L, Groysman M, et al. (2018). Astrocytic Activation Generates De Novo Neuronal Potentiation and Memory Enhancement. Cell 174, 59–71.e14. 10.1016/j.cell.2018.05.002. [PubMed: 29804835]
31. Tran T, Unal CT, Severin D, Zaborszky L, Rotstein HG, Kirkwood A, and Golowasch J (2019). Ionic current correlations are ubiquitous across phyla. Sci. Rep. 9, 1687. 10.1038/s41598-018-38405-6. [PubMed: 30737430]
32. Boric K, Muñoz P, Gallagher M, and Kirkwood A (2008). Potential adaptive function for altered long-term potentiation mechanisms in aging hippocampus. J. Neurosci. 28, 8034–8039. 10.1523/JNEUROSCI.2036-08.2008. [PubMed: 18685028]
33. White WE, and Hooper SL (2013). Contamination of current-clamp measurement of neuron capacitance by voltage-dependent phenomena. J. Neurophysiol. 110, 257–268. 10.1152/jn.00993.2012. [PubMed: 23576698]
34. Rall W (1977). Core conductor theory and cable properties of neurons. In Handbook of Physiology (Section 1, the Nervous System I, Cellular Biology of Neurons), Kandel ER, ed. (American Physiological Society), pp. 39–97.
35. Weiler S, Guggiana Nilo D, Bonhoeffer T, Hu€bener M, Rose T, and Scheuss V (2023). Functional and structural features of L2/3 pyramidal cells continuously covary with pial depth in mouse visual cortex. Cereb. Cortex 33, 3715–3733. 10.1093/cercor/bhac303. [PubMed: 36017976]

Highlights

- Neuronal membrane capacitance, C_m, is not highly stable, as often assumed
- C_m changes daily up to 2-fold in two types of glutamatergic cells
- In cortical parvalbumin$^+$ interneurons, C_m does not change
- C_m changes strongly affect the temporal window for integrating distinct synaptic inputs

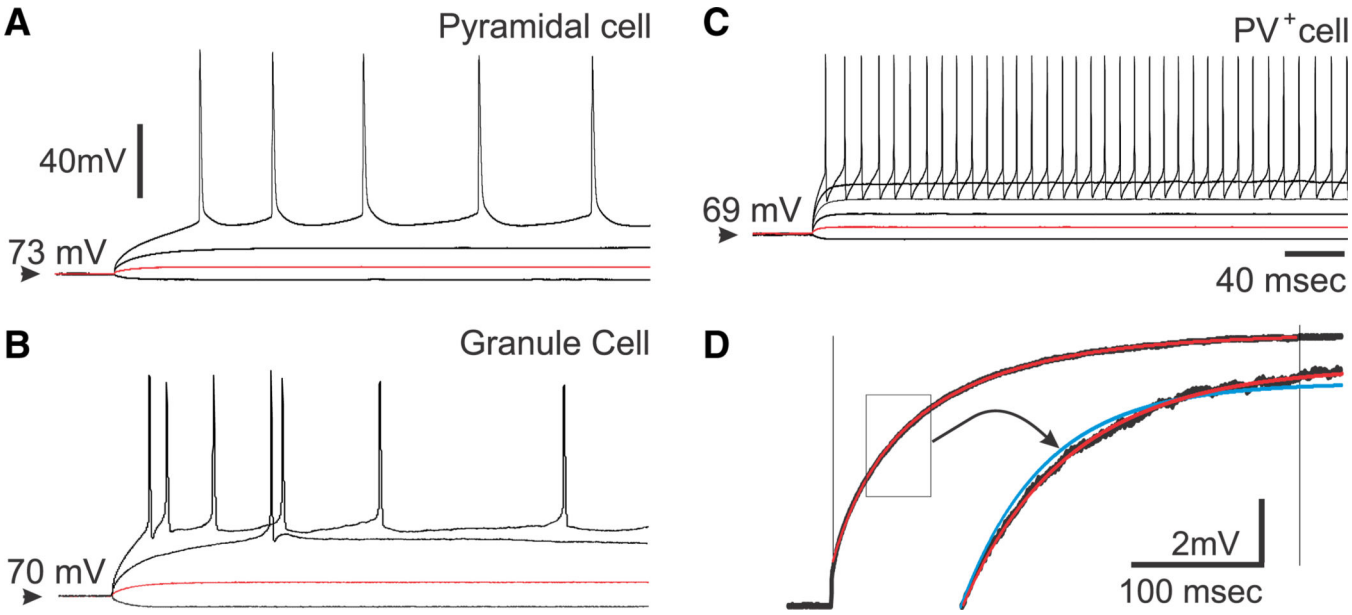

Figure 1. Typical neuronal activity of pyramidal cells, PV$^+$ cells, and GCs in response to current pulses

(A–C) Cortical pyramidal neurons (A) and hippocampal GCs (B) display a low frequency of action potential firing compared to cortical PV$^+$ cells (C). A range of current pulses was applied, and a subthreshold voltage response (red traces) in each case was fitted with a double exponential function from which membrane capacitance was derived, as described in STAR Methods.

(D) Example of a double exponential fit. The vertical lines indicate the limits for the 2-exponential fit (red trace) to a data trace (black). The boxed portion of the trace is shown amplified, with a 2-exponential fit (red trace) and a single exponential fit (blue trace) superimposed to illustrate the improved goodness of the fit with two over one exponential.

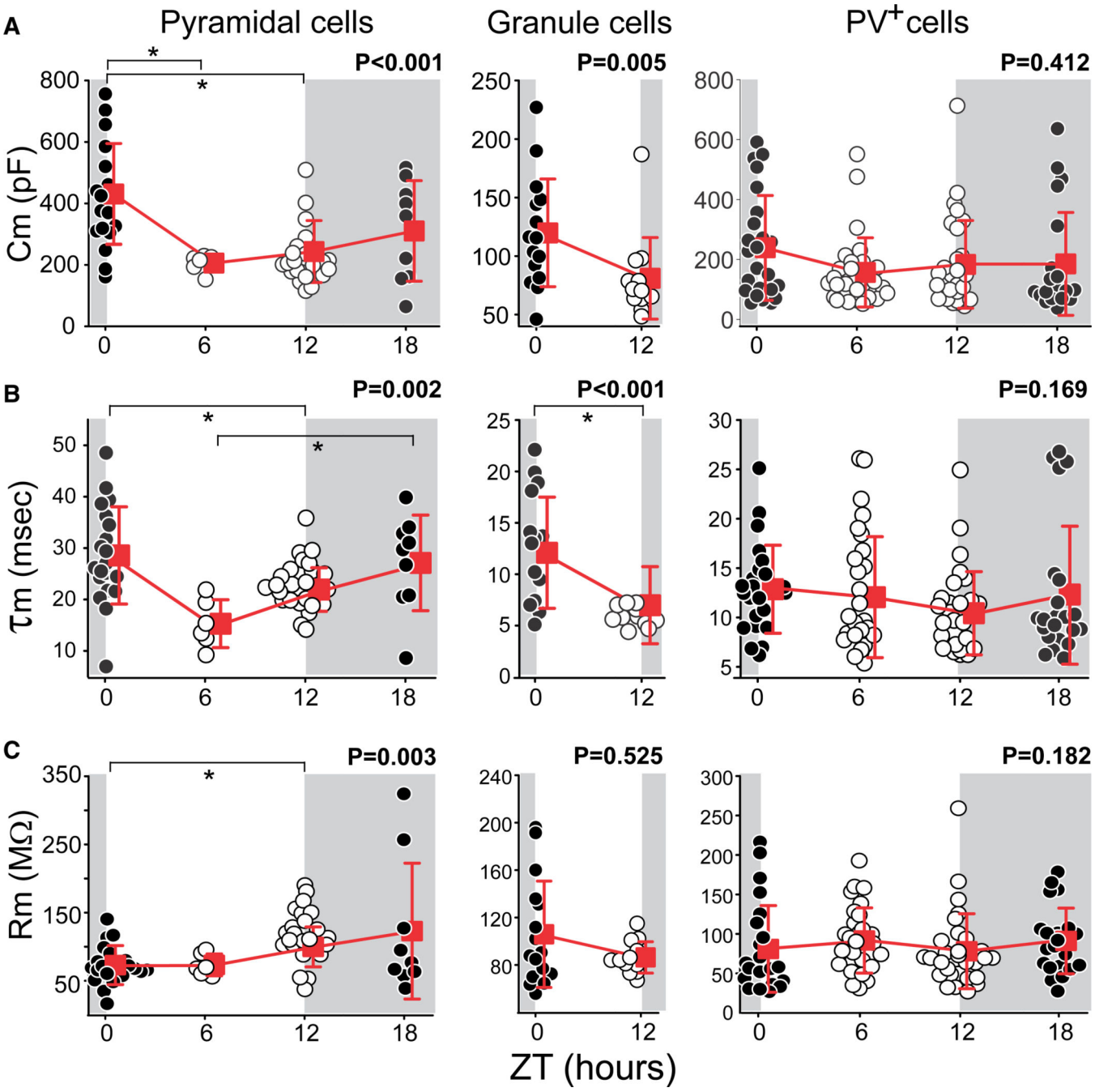

Figure 2. Changes with time of day of C_m, τ_m, and R_m

(A–C) C_m changes (A), τ_m changes (B), and R_m changes (C) of visual cortex layer 2/3 pyramidal cells (left), hippocampus GCs (center), and visual cortex inhibitory PV^+ cells (right). C_m of both excitatory neurons (cortical pyramidal and hippocampal GCs) are highest at ZT0 (dark phase, gray area) and lowest at ZT6–ZT12 (light phase, white area). τ_m tracks these changes of C_m and peaks at around ZT0, while R_m does not change significantly with time of day in either GCs or PV^+ cells. Only pyramidal cells show a significant change of R_m monotonically increasing with time of day. Average ± SD is shown as red squares and

connecting lines, slightly displaced from the individual data for clarity. Statistical details are listed in Tables S1–S3, but p values from one-way ANOVAs (pyramidal, PV^+ cells) and Student's t tests (GCs) are given here at the top right corners. Horizontal bars with vertical wings represent a post-hoc test ($*p < 0.05$) for the difference of the indicated pair.

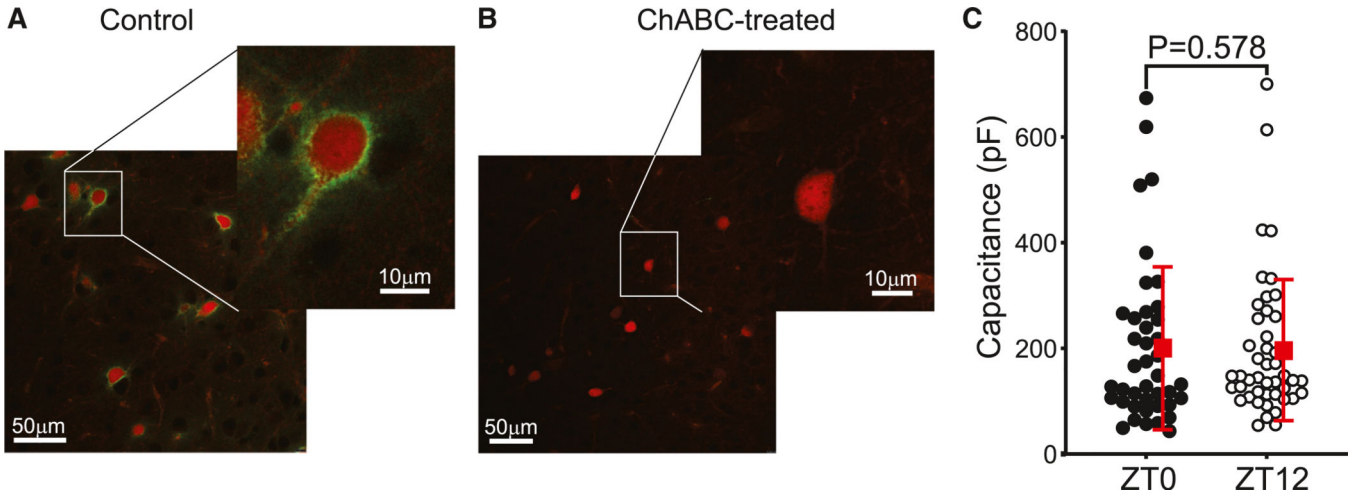

Figure 3. PNNs surrounding PV$^+$ neurons do not regulate daily C_m changes

(A) Confocal image of the V1 region of a mouse cortical slice (region in the white square magnified). All td-tomato expressing, red-stained PV$^+$ cells are clearly surrounded around the somata and proximal dendritic regions by a halo of WFA-positive material, indicative of the presence of a PNN.

(B) After 45 min of ChABC treatment, the WFA staining is nearly completely eliminated.

(C) The membrane capacitance of the individual ChABC-treated cells (black symbols for individual ZT0 and hollow symbols for individual ZT12 cells) and the average ± SD (slightly displaced red squares and whiskers) do not depend on ZT ($p = 0.578$, Student's t test). Note that the C_m values are not only indistinguishable between ChABC-treated ZT0 and ZT12 cells but also indistinguishable from the untread controls in Figure 2A.

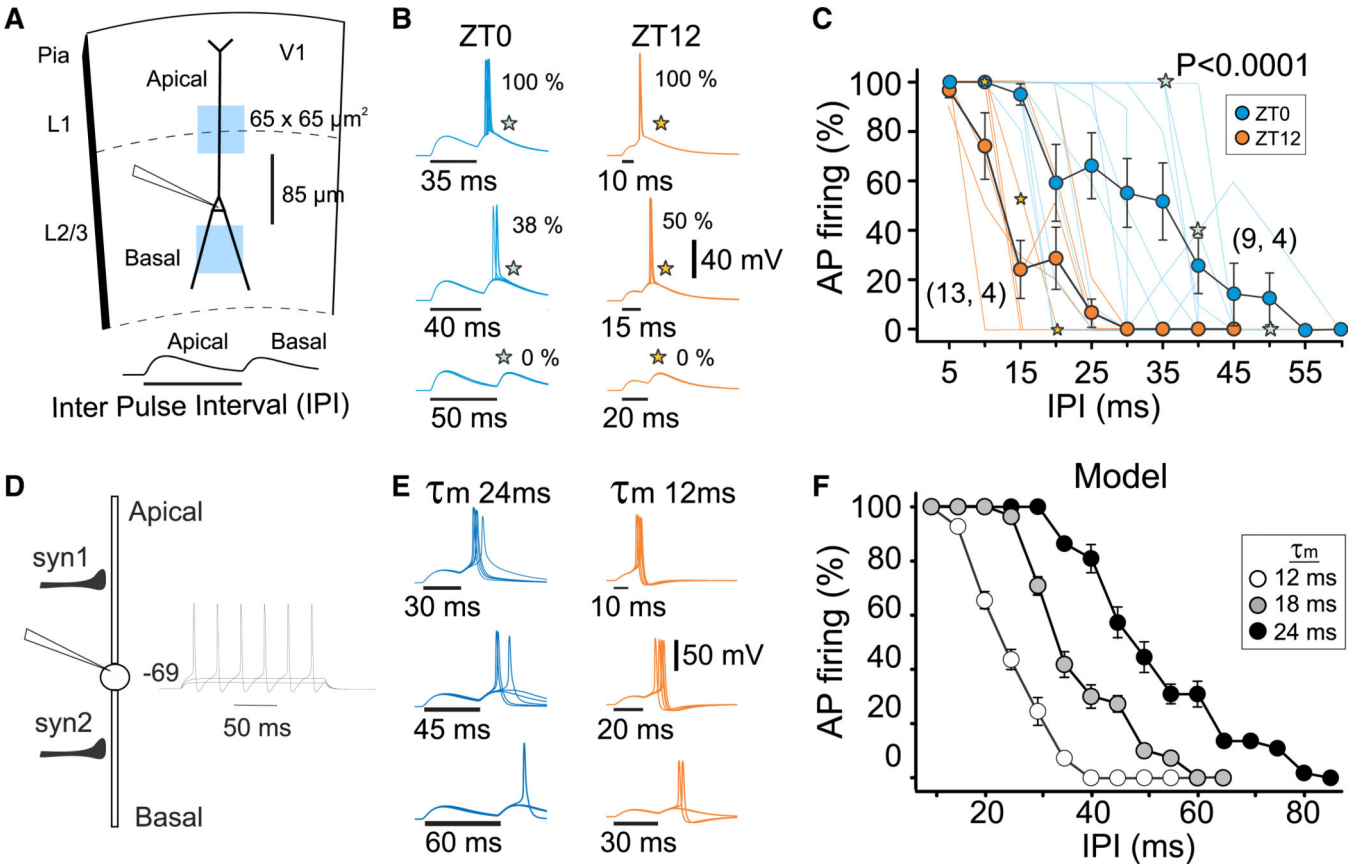

Figure 4. Synaptic integration is significantly affected by membrane capacitance changes

(A) Experimental setup. Two 65 × 65 µm squares of 470-nm-wavelength light pulses were sequentially applied (apical dendrite first) on approximately the center of the main apical and basal dendrites. The light intensity of each square pulse was adjusted to evoke a response at 80% of the spike threshold. The time between these pulses (IPI) was modified to be between 5 and 60 ms. The pulses were repeated several times, and the percentage of firing at each IPI was computed for each cell.

(B) Example responses of individual cells collected at ZT0 (blue) and ZT12 (orange). Indicated is the fraction of times that each particular cell fired action potentials at each IPI. Stars identify the points in (C).

(C) Summary graph of all experiments (9 cells at ZT0, 13 cells at ZT12, 4 mice each), showing that probability of firing decreases as the IPI increases, but more slowly and at higher IPIs in ZT0 cells, which has the largest C_m. Faint traces correspond to individual cells; stars label the points for which the voltage traces are shown in (B). Two-way ANOVA, $p < 0.0001$. Data are means ± SE of the means.

(D) Schematic of a simplified model pyramidal cell with activity in response to current pulses (STAR Methods).

(E) Examples of model cell runs (5 each) for models with time constants comparable to those in pyramidal cells at ZT0 (24 ms) and ZT12 (12–18 ms) with different IPIs.

(F) Graph summarizing the model's results for three different time constants, showing that cells with the largest C_m and, thus, τ_m integrate the two excitatory postsynaptic potentials over a wider window of IPIs. Data are means ± SE of the means.

KEY RESOURCES TABLE

REAGENT or RESOURCE	SOURCE	IDENTIFIER
Antibodies		
Wisteria Floribunda Lectin	Vector Laboratories, USA	Cat# FL-1351; RRID:AB_2336875
Chondroitinase ABC from Proteus vulgaris (ChABC)	Sigma-Adrich, St. Louis, USA	Cat# C3667
Bovine Serum Albumin	Fisher BioReagents, USA	Cat# 9048–46-8
Chemicals, peptides, and recombinant proteins		
ProLong™ Gold Antifade Mountant	Thermo Fisher Scientific, USA	RRID:SCR_015961
Experimental models: Organisms/strains		
PV-cre; Ai14 mice	Jackson Laboratories, Bar Harbor, Maine, USA	RRID:IMSR_JAX:008069
C57BL/6 mice	Jackson Laboratories, Bar Harbor, Maine, USA	RRID:IMSR_JAX:000664
Emx1-Cre mouse line	Jackson Laboratories, Bar Harbor, Maine, USA	RRID:IMSR_JAX:005628
Ai32 mouse line	Jackson Laboratories, Bar Harbor, Maine, USA	RRID:IMSR_JAX:012569
Software and algorithms		
SigmaPlot	Systat Software, Inc., San Jose, CA, USA	RRID:SCR_010285
CorelDraw	Corel Inc., Austin, TX, USA	RRID:SCR_014235
MATLAB 2023b	The Mathworks Inc. USA	NA
Model pyramidal cell	This paper	https://github.com/golowasch/Pyramidal_ball-2-sticks